Histidine → Carboxamide Ligand Substitutions in the Zinc Binding Site of Carbonic Anhydrase II Alter Metal Coordination Geometry but Retain Catalytic Activity†

Charles A. Lesburg,‡,§ Chih-chin Huang,|| David W. Christianson,*,‡ and Carol A. Fierke*,||

Department of Chemistry, University of Pennsylvania, Philadelphia, Pennsylvania 19104-6323, and Department of Biochemistry, Duke University Medical Center, Box 3711, Durham, North Carolina 27710

Received June 2, 1997; Revised Manuscript Received September 19, 1997⊗

ABSTRACT: The catalytic zinc ion of human carbonic anhydrase II (CAII) is coordinated by three histidine ligands (H94, H96, and H119) and a hydroxide ion with tetrahedral geometry. Structural and functional analysis of variants in which the zinc ligands H94 and H119 are substituted with asparagine and glutamine, and comparison with results obtained with aspartate and glutamate substitutions indicate that the neutral ligand field provided by the protein optimizes the electrostatic environment for the catalytic function of the metal ion, including stabilization of bound anions. This is demonstrated by catalytic activity measurements for ester hydrolysis and CO_2 hydration, as well as sulfonamide inhibitor affinity assays. High-resolution X-ray crystal structure determinations of H94N, H119N, and H119Q CAIIs reveal that the engineered carboxamide side chains coordinate to zinc with optimal stereochemistry. However, zinc coordination geometry remains tetrahedral only in H119Q CAII. Metal geometry changes to trigonal bipyramidal in H119N CAII due to the addition of a second water molecule to the zinc coordination polyhedron and also in H94N CAII due to the displacement of zinc-bound hydroxide by the bidentate coordination of a Tris molecule. Possibly, the bulky histidine imidazole ligands of the native enzyme play a role in disfavoring trigonal bipyramidal coordination geometry for zinc. Protein−metal affinity is significantly compromised by all histidine → carboxamide ligand substitutions. Diminished affinity may result from significant movements (up to 1 Å) of the metal ion from its position in the wild-type enzyme, as well as the associated, minor conformational changes of metal ligands and their neighboring residues.

Carbonic anhydrase II (CAII)[1] (EC 4.2.1.1) is a zinc metalloenzyme that catalyzes the reversible hydration of carbon dioxide (Silverman & Lindskog, 1988; Lindskog & Liljas, 1993; Christianson & Fierke, 1996). It is widely distributed in many cell types and involved in various physiological functions, including pH regulation, CO_2 and HCO_3^- transport, and water and electrolyte balance (Sly & Hu, 1995). The structure of CAII from human blood has been determined by X-ray crystallographic methods (Liljas et al., 1972) and refined at 1.54 Å resolution (Håkansson et al., 1992). The active site zinc ion is located at the bottom of a cavity 15 Å in depth where it is coordinated by three histidine ligands (N_ϵ of H94, N_ϵ of H96, and N_δ of H119) and a hydroxide ion with tetrahedral geometry. These zinc ligands are further hydrogen bonded to other protein groups to form a hydrogen bond network: the N_δ−H group of H94 is hydrogen bonded to the side chain carboxamide oxygen of Q92; the N_δ−H group of H96 is hydrogen bonded to the backbone amide carbonyl of N244; the N_ϵ−H group of H119 is hydrogen bonded to the carboxylate of E117; and zinc-bound hydroxide donates a hydrogen bond to the hydroxyl of T199, which in turn donates a hydrogen bond to the carboxylate of E106 (Figure 1).

The CAII-catalyzed CO_2 hydration reaction occurs in two distinct steps, as shown in Scheme 1 (Silverman & Lindskog, 1988; Silverman, 1995). In the first step, zinc-bound hydroxide attacks the carbonyl carbon of CO_2 to form zinc-bound bicarbonate (Coleman, 1967; Lindskog & Coleman, 1973); bicarbonate is subsequently displaced by a ligand-exchange step with water. In CAII, the second-order rate constant for CO_2 hydration approaches the diffusion-controlled limit, with $k_{cat}/K_M \approx 10^8$ M^{-1} s^{-1}. In the second step, a proton is transferred from zinc-bound water to buffer via shuttle group H64 to regenerate the catalytically active species, zinc-bound hydroxide (Steiner et al., 1975; Tu et al., 1989). The intramolecular proton transfer step is rate-limiting for CO_2 hydration at high buffer concentrations (Jonsson et al., 1976; Steiner et al., 1975).

In CAII, the protein scaffolding modulates the chemical properties of the zinc ion and zinc-bound solvent. Specifically, the protein plays a critical role in lowering the pK_a

† This work was supported by the Office of Naval Research and the National Institutes of Health (GM40602); C.A.L. is supported in part by NIH Cell and Molecular Biology Training Grant GM07229. Additionally, C.A.F. gratefully acknowledges the receipt of an American Heart Association Established Investigator Award.

* Authors to whom correspondence should be addressed.

‡ University of Pennsylvania.

§ Current address: Structural Chemistry Department, Schering-Plough Research Institute, 2015 Galloping Hill Road, Kenilworth, NJ 07033.

|| Duke University Medical Center.

⊗ Abstract published in *Advance ACS Abstracts,* December 1, 1997.

[1] Abbreviations: AZA, acetazolamide; CAII, human carbonic anhydrase II; CHES, 2-(*N*-cyclohexylamino)ethanesulfonic acid; EDTA, (ethylenedinitrilo)tetraacetic acid; DNSA, dansylamide; H94N, CAII variant with asparagine substituted for histidine-94, etc., using the one-letter amino acid code; MES, 2-(*N*-morpholino)ethanesulfonic acid; MOPS, 3-(*N*-morpholino)propanesulfonic acid; PNPA, *p*-nitrophenyl acetate; TAPS, *N*-[tris(hydroxymethyl)methyl]-3-aminopropanesulfonic acid; Tris, tris(hydroxymethyl)aminomethane.

S0006-2960(97)01296-8 CCC: $14.00

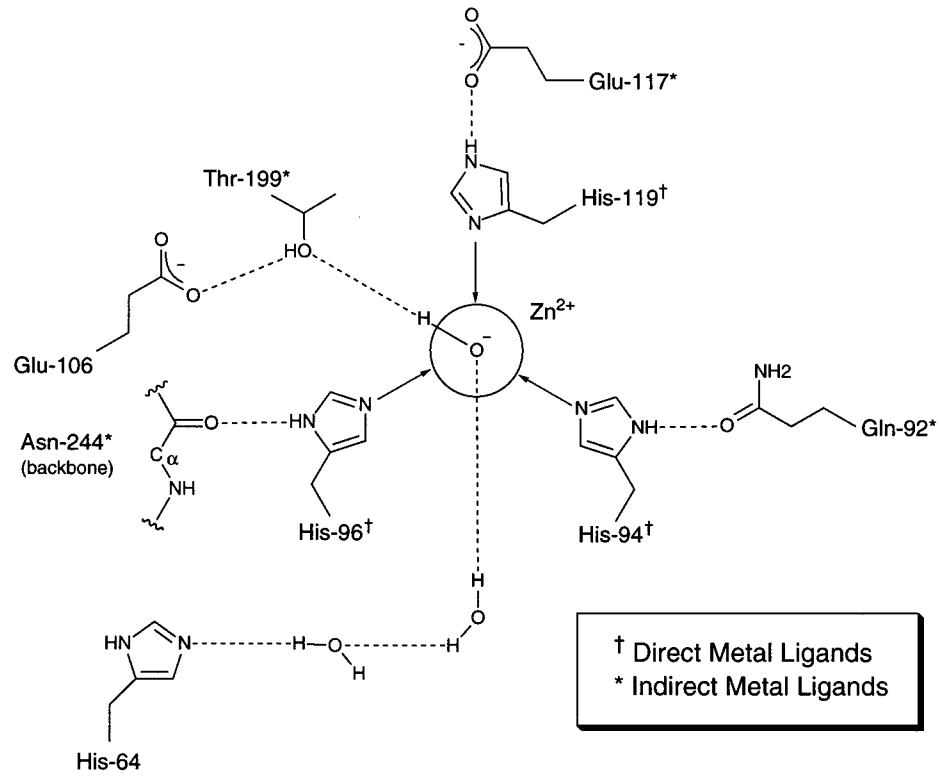

FIGURE 1: Scheme of the zinc binding site of native CAII.

Scheme 1

$$EZn\text{-}OH^- + CO_2 \rightleftharpoons EZn\text{-}HCO_3^- \overset{H_2O}{\rightleftharpoons} EZn\text{-}OH_2 + HCO_3^-$$

$$\underset{H64}{EZn\text{-}OH_2} \rightleftharpoons \underset{H64H^+}{EZn\text{-}OH^-} + Buffer \rightleftharpoons \underset{H64}{EZn\text{-}OH^-} + BufferH^+$$

of zinc-bound water to 6.8 from 10 in solution (Woolley, 1975) and increasing the second-order rate constant for CO_2 hydration by more than 10^4-fold (Coleman, 1984). Structure-based dissection of the zinc binding site of CAII, including modification of the direct ligands (Alexander et al., 1993; Kiefer et al., 1993; Ippolito & Christianson, 1994; Kiefer & Fierke, 1994; Xue et al., 1994; Ippolito et al., 1995) and the indirect ligands (Kiefer et al., 1995; Lesburg & Christianson, 1995; Huang et al., 1996), suggests that the electrostatic environment of zinc is a principal feature governing the chemical properties of the metal site. In particular, substitution of negatively charged groups for neutral histidine ligands significantly increases the pK_a of zinc-bound water while simultaneously decreasing its reactivity (Kiefer & Fierke, 1994). In fact, the hydrase and esterase activities of a number of variants are inversely proportional to the pK_a of zinc-bound water, suggesting that electrostatic stabilization of the transition state by the positively charged zinc ion is a dominant factor in catalysis (Christianson & Fierke, 1996).

In this work, we further probe the electrostatic and structural features of the zinc site in CAII by making *neutral* amino acid substitutions for histidine zinc ligands. Replacing the imidazole side chain of histidine with the carboxamide side chains of asparagine or glutamine—neutral amino acids that are isosteric with aspartate and glutamate—can possibly maintain metal coordination and preserve the neutral electrostatic environment of the ligand field provided by the protein scaffolding. Here, we demonstrate that single-point substitutions of asparagine or glutamine for the histidine ligands in CAII destabilize zinc-bound hydroxide and ionized sulfonamide inhibitors significantly less than the corresponding isosteric substitutions of aspartate or glutamate. Furthermore, the CO_2 hydrase activities of asparagine or glutamine zinc site variants are higher than the corresponding activities measured for aspartate and glutamate variants. These results indicate that the neutral ligand field of native CAII is crucial for high catalytic efficiency at neutral pH.

Although the carbonyl oxygen of the carboxamide side chain of asparagine or glutamine may coordinate to zinc, such an interaction is expected to be weaker than that achieved by the side chains of histidine, aspartate, or glutamate with a comparable zinc−ligand separation (Gurd & Wilcox, 1956). Nevertheless, transition metal coordination by a carboxamide oxygen is occasionally observed in native enzymes such as kidney bean purple acid phosphatase [a Fe(III)−Zn(II) metalloenzyme; Sträter et al., 1995] and serine/threonine protein phosphatase-1 [a Mn(II)−Mn(II) metalloenzyme; Goldberg et al., 1995]. Intriguingly, substitution of a histidine ligand by asparagine or glutamine weakens metal affinity, but only modestly decreases the catalytic activity of cytidine deaminase (Smith et al., 1994), arginase (Cavalli et al., 1994; Scolnick et al., 1997), and alkaline phosphatase (Ma & Kantrowitz, 1994, 1996; Ma et al., 1995). X-ray crystal structures of the arginase and alkaline phosphatase variants reveal that the engineered carboxamide side chain does not coordinate to the metal ion (no crystallographic data are available for the cytidine deaminase variant). Therefore, the crystal structure determinations of H94N (with and without bound sulfonamide inhibitor), H119N, and H119Q CAIIs demonstrate that asparagine or glutamine side chains can coordinate zinc with optimal stereochemistry as a substitute for histidine; however, protein−zinc affinity is severely compromised. Surprisingly, the structures of H94N and H119N CAIIs reveal a novel

change in zinc coordination geometry from tetrahedral to trigonal bipyramidal because of the displacement of zinc-bound hydroxide by Tris in the former variant and the addition of a second water molecule to the zinc coordination polyhedron of the latter variant.

MATERIALS AND METHODS

Preparation of H119N, H119Q, H94N, and H94Q CAII Variants. The CAII variants were produced using oligonucleotide-directed mutagenesis of the cloned human CAII gene in pCAM (Kunkel et al., 1985; Krebs et al., 1993) by replacing the H94 or H119 (CAC) codon with asparagine (AAC/T) or glutamine (CAA/G), and the entire CAII gene of the variants was sequenced (Sanger et al., 1977). CAII was induced by the addition of 0.25 mM isopropyl β-D-thiogalactopyranoside to mid-log *Escherichia coli* BL21-(DE3)pCAM cells followed by incubation at 30 °C for 5 h and then purified by sequential chromatography on DEAE-Sephacel and S-Sepharose media (Alexander et al., 1993). Acetazolamide-complexed H94N CAII was prepared by elution from sulfonamide affinity resin with acetazolamide (Osborne & Tashian, 1975). The protein concentration was determined by absorbance using $\epsilon_{280} = 54\,000$ M^{-1} cm^{-1} determined for wild-type CAII (Tu & Silverman, 1982).

Catalytic Activity. The initial rate of *p*-nitrophenyl acetate (PNPA) hydrolysis catalyzed by CAII was monitored by absorbance, $\epsilon_{348} = 5000$ M^{-1} cm^{-1} (Armstrong et al., 1966). The reaction was assayed under k_{cat}/K_M conditions at 0.5−2 μM CAII variants, 0.5 mM PNPA in 50 mM buffer, either MES (pH 6.0−6.5), MOPS (pH 7.0−7.5), TAPS (pH 8.0−8.5), or CHES (pH 9.0−10.0), with the ionic strength held constant at 0.1 M with Na_2SO_4. Background rates were measured in the presence of 0.1 mM acetazolamide. Inhibition of the esterase activity of H94N CAII was measured at pH 9.0 in 50 mM CHES buffer with varying TAPS (0−100 mM) or Tris (0−50 mM) concentrations. The pK_a values of the CAII variants were obtained by fitting the data to eq 1, and inhibition constants were determined by fitting the data to eq 2 using the curve-fitting program Kaleidagraph (Synergy Software).

$$(k_{cat}/K_M)_{obs} = \frac{k_{cat}/K_M}{1 + 10^{(pK_a - pH)}} \quad (1)$$

$$(k_{cat}/K_M)_{obs} = \frac{k_{cat}/K_M}{1 + [I]/K_i} \quad (2)$$

Initial rates of CO_2 hydration were measured by the changing pH-indicator method (Khalifah, 1971) in a KinTek stopped-flow apparatus using the following conditions: 0−24 mM CO_2, 0.2−5 μM CAII variants at 25 °C, and either 25 μM *m*-cresol purple, 50 mM TAPS, pH 9.0, or 25 μM *p*-nitrophenol, 50 mM MOPS, pH 7.6−7.9, with the ionic strength maintained at 0.1 M with Na_2SO_4. Background rates measured in the absence of CAII were subtracted from the observed rates. Inhibition of CO_2 hydrase activity by Tris and TAPS was measured at 6−24 mM CO_2, 1 μM H94N CAII, 25 μM *m*-cresol purple, 50 mM CHES, pH 9.0, 25 °C, ionic strength held at 0.1 M with Na_2SO_4, and varying concentrations of Tris (0−2 mM) or TAPS (0−80 mM).

Zinc Dissociation Rate and Equilibrium Constant. All solutions were prepared in plasticware using deionized water and buffers treated with Chelex-100 resin (Sigma). Free zinc was removed from CAII variants by chromatography on a Sephadex G-25M column (PD-10, Pharmacia). The rate constant for zinc dissociation, k_{off}, was determined by diluting CAII variants (0.1−10 μM) into an assay buffer consisting of 0.5 mM PNPA, 10 mM MOPS, pH 7.0, with 5 mM EDTA to chelate zinc dissociating from the enzyme. Dissociation of zinc from CAII was monitored by the time-dependent decrease in the PNPA esterase activity, reflecting the concentration of enzyme-bound zinc. This decrease is not dependent on the concentration of EDTA. The k_{off} is calculated by fitting the data to eq 3, where $[P]_t$ represents the formation of *p*-nitrophenol at each time point, and $(activity)_{t=0}$ is the initial activity of the zinc-bound enzyme assayed in the absence of EDTA.

$$[P]_t = \frac{(activity)_{t=0}}{k_{off}}(1 - e^{-k_{off}t}) \quad (3)$$

To measure the zinc dissociation constant, K_{Zn}, 0.2 mL of CAII variants (≈60 μM) was dialyzed against 500 mL of zinc/dipicolinate metal ion buffers (0−85 μM total zinc/0.1−2 mM dipicolinate) in 10 mM MOPS, pH 7.0. After the samples were incubated for 9−24 h at 30 °C, the enzyme concentration ($[E]_{tot}$) was determined by absorbance at 280 nm. The total zinc concentration in the dialysate and enzyme sample was measured by absorbance at 500 nm in the presence of 0.1 mM 4-(2-pyridylazo)resorcinol and 4 M guanidine hydrochloride compared to a standard curve (Kiefer & Fierke, 1994; Hunt et al., 1977; Hunt et al., 1984). The concentration of enzyme-bound zinc ([E·Zn]) was determined from the difference in the total zinc concentration between the two samples. Alternatively, the fraction of zinc-bound enzyme, $[E·Zn]/[E]_{tot}$, was determined from the relative specific activity for PNPA hydrolysis using the following assay buffers: 50 mM TAPS, pH 8.5 (H119N, H119Q), 50 mM MOPS, pH 8.4 (H94N), and 50 mM TAPS, pH 9.4 (H94Q). The concentration of free zinc was calculated from the dipicolinate−zinc stability constants (Sillén & Martell, 1964). The dissociation constants were calculated using the Kaleidagraph 3.0 (Synergy Software) curve-fitting program with eq 4 where C ranged from 0.9 to 1.1.

$$\text{relative activity} = \frac{[E·Zn]}{[E]_{tot}} = \frac{C}{1 + K_{Zn}/[Zn]_{free}} \quad (4)$$

Sulfonamide Dissociation Constants. Dansylamide (DNSA) dissociation constants were determined by measuring an increase in fluorescence (excitation = 280 nm, emission = 470 nm) upon binding DNSA to CAII (Nair et al., 1995; Chen & Kernohan, 1967) at 25 °C in 50 mM MOPS, pH 7.9. In some cases, the concentration of enzyme (1 μM) was comparable to the dissociation constant; therefore, the DNSA dissociation constants were calculated using eq 5, where Fl is the observed fluorescence, IF is the initial fluorescence, $[E]_t$ is the total enzyme concentration, $[D]_t$ is the total concentration of DNSA, and K_D is the dissociation constant for DNSA. Acetazolamide (AZA) binding was assayed by competition with bound DNSA as a decrease in fluorescence (excitation = 280 nm, emission = 470 nm). These titrations contained 1 μM CAII variants, DNSA (5−50 μM), 50 mM MOPS, pH 7.9, 25 °C, and varied

Table 1: Crystallographic Data Collection and Refinement Statistics

CAII variant (complex)	H119N	H119Q	H94N (Tris)	H94N (AZA)
no. of crystals	1	1	1	1
no. of measured reflections	73412	22514	45669	50903
no. of unique reflections	19942	11825	16217	19350
minimum resolution (Å)	20.0	20.0	20.0	20.0
maximum resolution (Å)	1.85	2.2	2.0	1.9
completeness of data overall (last 0.05 Å shell) (%)	92.7 (81.0)	93.8 (93.0)	95.4 (70.3)	97.5 (89.0)
R_{sym} overall (last shell)[a]	0.074 (0.236)	0.088 (0.318)	0.067 (0.223)	0.063 (0.375)
no. of reflections used in refinement (in test set)	18 815 (957)	11 074 (597)	15 259 (777)	18 626 (564)
R_{cryst} (R_{free})[b]	0.170 (0.230)	0.182 (0.249)	0.154 (0.207)	0.177 (0.219)
no. of water molecules in final cycle of refinement	181	38	137	49
RMS deviation from ideal bond lengths (Å)	0.009	0.012	0.007	0.007
RMS deviation from ideal bond angles (deg)	1.6	1.7	1.5	1.5
RMS deviation from ideal dihedral angles (deg)	25.4	25.6	25.1	25.2
RMS deviation from ideal improper angles (deg)	1.4	1.6	1.3	1.3

[a] R_{sym} for replicate reflections, $R = \sum|I_h - \langle I_h\rangle|/\sum\langle I_h\rangle$; I_h = intensity measured for reflection h; $\langle I_h\rangle$ = average intensity for reflection h calculated from replicate data. [b] Crystallographic R-factor, $R_{cryst} = \sum||F_o| - |F_c||/\sum|F_o|$, for reflections in the working set. Free R factor, $R_{free} = \sum||F_o| - |F_c||/\sum|F_o|$, for reflections in the test set. $|F_o|$ and $|F_c|$ are the observed and calculated structure factor amplitudes, respectively.

concentrations of AZA (0−180 μM). The AZA dissociation constant was calculated from these data using eq 6, where K_{AZA} is the dissociation constant for acetazolamide. In these titrations [DNSA] ≈ $[DNSA]_{tot}$ and the $[AZA]_{free}$ was calculated using eq 7.

$$\text{fraction Fl} = \frac{\text{Fl} - \text{IF}}{\text{EP} - \text{IF}} = \frac{([E]_t + [D]_t + K_D) - \sqrt{([E]_t + [D]_t + K_D)^2 - 4[E]_t[D]_t}}{2[E]_t} \quad (5)$$

$$\text{fraction Fl} = \frac{\text{Fl} - \text{EP}}{\text{IF} - \text{EP}} = \frac{1}{1 + (K_D/[DNSA])(1 + [AZA]/K_{AZA})} \quad (6)$$

$$[AZA]_{free} = [AZA]_{tot} - [E{\cdot}AZA] = [AZA]_{tot} - [E]_{tot} + [E{\cdot}DNSA] + [E] \quad (7)$$

Crystallography. H94N, H119N, and H119Q CAIIs were crystallized using the sitting drop method: 5−10 μL drops of precipitant buffer containing 50 mM Tris-HCl (pH 8.0 at 25 °C) and 2.0−2.5 M $(NH_4)_2SO_4$ were added to 5−10 μL drops containing approximately 10 mg/mL protein in the crystallization well. The outer well contained 1 mL of precipitant buffer. Crystals grew as very thin plates within 2 weeks at 4 °C; accordingly, up to 10 mM *n*-hexyl β-D-glucopyranoside was included in the crystallization wells to facilitate the formation of larger single crystals suitable for X-ray diffraction analysis (McPherson et al., 1986). Crystals were isomorphous with those of the native blood and recombinant wild-type enzymes and belonged to monoclinic space group $P2_1$ with unit cell parameters a = 42.7 Å, b = 41.7 Å, c = 73 Å, and β = 104.6° (Liljas et al., 1972; Alexander et al., 1991). Crystals of the H94N CAII−acetazolamide complex were prepared by crystallizing protein eluted from the sulfonamide affinity column with acetazolamide during the purification procedure.

Crystals were mounted in 0.7 mm diameter glass capillaries with a small portion of mother liquor and sealed with wax. Intensity data were collected on an R-AXIS IIc image plate detector. Individual ϕ oscillation images spanning 2° were collected for 15 min each for a total sweep of 120°. A Rigaku RU-200HB rotating anode X-ray generator provided Cu Kα radiation at 50 kV/100 mA (λ = 1.5418 Å). The crystal-to-detector distance was set to 90−100 mm and the detector swing angle (2θ) was set to 0°. The crystal orientation matrix was initially obtained using REFIX (Kabsch, 1993), and reflections were subsequently integrated with MOSFLM (Nyborg & Wonacott, 1977). Data reduction was completed using the CCP4 suite of programs (French & Wilson, 1978; Collaborative Computational Project No. 4, 1994).

The starting coordinate set for the refinement of each variant CAII structure was that of native CAII (Håkansson et al., 1992) with the atoms of the variant side chain and all water molecules deleted from the model. Each structure was refined by simulated annealing ($T_{initial}$ = 3000 K) with energy minimization as implemented in X-PLOR (Brünger et al., 1987). After initial rounds of refinement, electron density for each variant side chain was clear and unambiguous. The variant side chain and water molecules (and inhibitors in the Tris and acetazolamide complexes of H94N CAII) were modeled into electron density maps generated with Fourier coefficients $2|F_o| - |F_c|$ and $|F_o| - |F_c|$ and phases calculated from the in-progress atomic model. This work required the graphics software O (Jones et al., 1991), installed on a Silicon Graphics workstation.

During the refinement of each CAII variant, electron density maps were periodically calculated from the in-progress atomic model, and only minimal manual adjustments of atomic coordinates were found to be necessary. The application of a bulk solvent model as implemented in X-PLOR achieved a significant decrease in the crystallographic R-factor and the free R-factor. Refinement ultimately yielded structures with final crystallographic R-factors of 0.154−0.182 and excellent stereochemistry (Table 1). The RMS error in atomic positions for all CAII variants was estimated to be 0.2−0.3 Å using SIGMAA (Read, 1986). Each engineered carboxamide group coordinated to zinc with optimal coordination stereochemistry and separation, and zinc−ligand separations are recorded in Table 2. Electron density maps and coordinate superpositions shown in the figures were generated using MINIMAGE (Arnez, 1994) and MOLSCRIPT (Kraulis, 1991).

Table 2: Zinc−Ligand Distances in Histidine → Carboxamide and Histidine → Carboxylate CAII Zinc Site Variants

ligand	native	H119N	H119D	H119Q	H94N (Tris)	H94N (AZA)	H94D
His-94	2.1	2.0	2.2	2.1	2.0	2.0	2.1
His-96	2.1	2.0	2.0	2.0	2.1	2.0	2.4
His-119	2.1	2.3	2.8	1.9	2.1	2.0	2.2
SOL1	2.1	2.1	2.2	2.3			2.4
SOL2		2.2	2.4			2.9	2.6
Tris (O)					2.4		
Tris (N)					2.3		
AZA (N)	1.9[a]					2.1	

[a] From Vidgren et al. (1990).

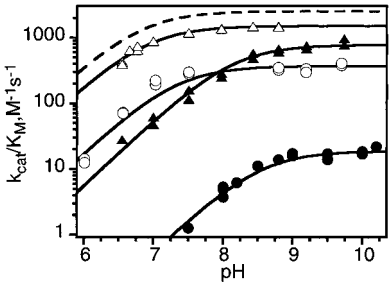

FIGURE 2: pH dependence of PNPA esterase activity of H119N CAII (▲), H119Q CAII (△), H94N CAII (○), H94Q CAII (●), and wild-type CAII (dashed line). The initial rate of *p*-nitrophenyl acetate (PNPA) hydrolysis was monitored by absorbance, $\epsilon_{348} = 5000\ M^{-1}\ cm^{-1}$ under k_{cat}/K_M conditions at 0.5−2 μM CAII variants, 0.5 mM PNPA in 50 mM buffer, either MES (pH 6.0−6.5), MOPS (pH 7.0−7.5), TAPS (pH 8.0−8.5), or CHES (pH 9.0−10.0), with the ionic strength held constant at 0.1 M with Na_2SO_4. The pK_a values of the CAII variants were obtained by fitting the data to eq 1.

RESULTS AND DISCUSSION

Structure and Esterase Activity. To delineate the effect of the electrostatic environment of the zinc ligands on the reactivity and pK_a of the zinc-bound solvent molecule, we measured the pH dependence of the second-order rate constant for hydrolysis of PNPA catalyzed by the H94N, H94Q, H119N, and H119Q CAII variants. As observed for wild-type CAII, the pH dependence of the esterase activity of each variant is consistent with the ionization of a single enzymic group (Figure 2, Table 3). The pH dependence of the esterase activity of wild-type CAII, and likely these variants as well, directly reflects the ionization of the zinc-bound water (Coleman, 1967; Lindskog & Coleman, 1973). Except for H94Q CAII, which is the least active variant with a 130-fold decrease in k_{cat}/K_M, substitution of a single histidine imidazole side chain with the carboxamide group of asparagine or glutamine reduces the pH-independent esterase activity only moderately (2−7-fold; Table 3). In the remaining discussion of this section, we correlate the activities of these variants with their X-ray crystal structures, focusing first on asparagine variants and subsequently on glutamine variants.

The pH-independent esterase activities of CAII variants containing a neutral histidine → asparagine substitution are comparable to those containing the corresponding negatively charged histidine → aspartate substitution (Kiefer & Fierke, 1994; Table 3). This comparison suggests that the modest decreases in esterase activity resulting from these substitutions most likely reflect structural changes in the active site resulting from histidine → aspartate or histidine → asparagine substitutions, rather than solely from changes in the electrostatic environment. X-ray crystallographic analysis of these variants suggests that the principal structural change responsible for the activity loss is the movement of the active site zinc ion, as well as alternative zinc coordination geometries. The crystal structure of H94D CAII reveals a distorted tetrahedral zinc coordination polyhedron; however, the zinc ion moves nearly 1 Å in order to maintain a coordination interaction with the shorter D94 side chain, and changes in the binding mode of the nonprotein zinc ligand are suggestive, but not conclusively so, of a partially occupied zinc-bound Tris molecule (Kiefer et al., 1993). The electron density map of the H94N CAII active site conclusively reveals that the engineered carboxamide side chain coordinates to zinc in a trigonal bipyramidal coordination polyhedron, in which two nonprotein ligands are supplied by the primary amino group and one hydroxyl group of the buffer Tris (Figure 3). The Tris molecule is additionally stabilized by hydrogen bond interactions between its hydroxyl groups and the side chain amide group of N94, T199 (both main chain nitrogen and side chain hydroxyl group), and T200 (side chain hydroxyl group). Additionally, the zinc ion moves 0.8 Å toward the variant side chain from its position in the native enzyme. A comparison of the structures of H94D and H94N CAIIs is found in Figure 4.

Apart from minor conformational changes of the remaining protein−zinc ligands which optimize zinc coordination interactions, and the observation of both "in" and "out" conformations of H64 (as observed in the native structure; Håkansson et al., 1992), no other significant structural changes are observed in the active sites of H94D or H94N CAIIs. If the active site zinc ions of these variants retain trigonal bipyramidal coordination geometries in the absence of Tris, it is possible that the comparable decreases in esterase activities measured for these variants result from similar changes in the coordination geometry of zinc and the position of zinc-bound solvent.

Given that the crystal structure of H94N CAII reveals a fully occupied Tris molecule coordinated to the active site metal ion through a bidentate coordination interaction and stabilized by the side chain amide group of N94, it is not surprising that the esterase activity of this variant decreases as the concentration of buffer, either Tris or TAPS, increases (data not shown). At pH 9, the observed inhibition constants (eq 2) are 0.04 ± 0.01 and 4.0 ± 0.7 mM for Tris and TAPS, respectively. Tris and TAPS also inhibit the CO_2 hydrase activity of H94N CAII with slightly lower inhibition constants, K_i(Tris) = 0.012 ± 0.002 mM and K_i(TAPS) = 1.3 ± 0.2 mM at 24 mM CO_2, pH 9.0. Neither wild-type CAII nor any of the other carboxamide-substituted CAII variants are inhibited by these buffers.

The electron density map of the H119N CAII active site reveals that the engineered carboxamide side chain coordinates to zinc; additionally, metal coordination geometry is trigonal bipyramidal due to the introduction of a second solvent molecule to the zinc coordination polyhedron (Figure 5). This requires a slight movement of the zinc ion from its position in the native enzyme (~0.2 Å). No other significant structural changes are observed in the active site of this variant, and both of the zinc-bound solvent molecules maintain possible hydrogen bond interactions with Thr-199 (SOL1-T199 O_γ separation = 2.9 Å; SOL2-T199 O_γ separation = 3.2 Å).

Table 3: Steady-State Kinetic Parameters for PNPA Hydrolysis and Dissociation Constants for Sulfonamide Inhibitors

CAII	k_{cat}/K_M[a] (M^{-1} s^{-1})	pK_a[a]	K_{AZA}[b] (μM)	K_D[c] (μM)
wild-type[d]	2500 ± 200	6.8 ± 0.1	0.006 (0.0057)[e]	1.2
H94N	370 ± 30	7.3 ± 0.2	0.002 ± 0.001 (0.0016)	0.2 ± 0.1
H94Q	20 ± 5	8.5 ± 0.2	0.25 ± 0.2 (0.05)	3.3 ± 1.3
H94D[f]	365	≥9.6	207 (5.1)	
H94E[f]	≤2		560	
H94C[f]	117	≥9.5	55 (1.7)	
H119N	770 ± 70	8.1 ± 0.2	0.028 ± 0.010 (0.011)	1.8 ± 0.5
H119Q	1490 ± 120	6.9 ± 0.2	0.23 ± 0.10 (0.21)	15.2 ± 7.9
H119D[f]	830	8.6	2.4 (0.5)	
H119E[g]	20 ± 10			

[a] pK_a and pH-independent k_{cat}/K_M calculated using eq 1 as described in the legend of Figure 2. [b] K_{AZA} for acetazolamide measured in 50 mM MOPS, pH 7.9, 25 °C, and calculated using eqs 5−7. [c] K_D for dansylamide measured in 50 mM MOPS, pH 7.9, 25 °C, and calculated using eq 5. [d] Taken from Fierke et al. (1991). [e] The dissociation constant corrected for the pK_a of the zinc−water is shown in parentheses; $K_{D\,corr} = K_{D\,obs}/(1 + 10^{pK_a - pH})$. [f] Taken from Kiefer and Fierke (1994). [g] Measured in 50 mM TAPS, pH 9.0, 25 °C. H119E CAII precipitates at pH ≤7.5; therefore, the pK_a cannot be determined.

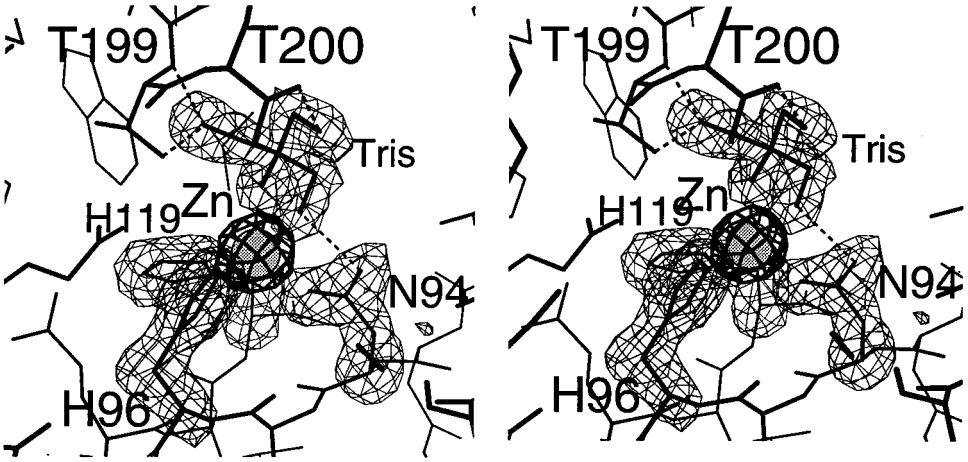

FIGURE 3: Difference electron density map of H94N CAII, generated with Fourier coefficients $|F_o| - |F_c|$ and phases calculated from the final model less the atomic coordinates of zinc ligands N94, H96, H119, and zinc-bound Tris. The map is contoured at 3.5σ (thin lines); refined atomic coordinates are superimposed. Note that the buffer molecule Tris coordinates to zinc through its amino nitrogen and one hydroxyl oxygen, thereby changing zinc coordination geometry to trigonal bipyramidal. Tris binding is also stabilized by hydrogen bond interactions (dashed lines) with the side chains of N94, T199, and T200, and the backbone NH group of T199. This binding mode accounts for the unique inhibitory activity of Tris against H94N CAII. The thick lines represent a difference map omitting the zinc ion from the structure factor calculation and contoured at 10σ.

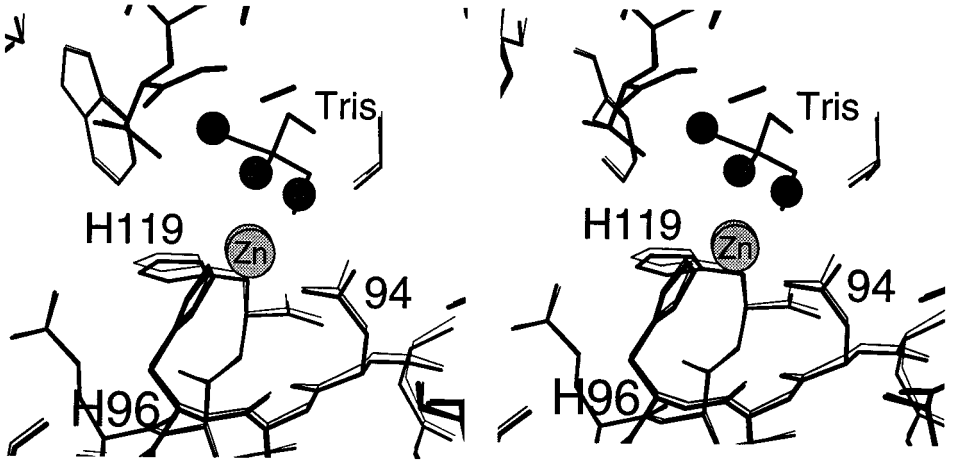

FIGURE 4: Least-squares superposition of the zinc binding sites of H94D CAII (thin lines; Ippolito & Christianson, 1994) and H94N CAII (thick lines). Intriguingly, in the H94N CAII structure two hydroxyl oxygen atoms and the amino nitrogen atom of the Tris buffer molecule are located near positions of well-ordered solvent molecules (spheres) observed in the H94D CAII structure (Kiefer et al., 1993).

Comparison of the structures of native, H119N, and H119D CAIIs (Kiefer et al., 1993) reveals that solvent atom positions change to accommodate the alteration of metal coordination geometry from tetrahedral to trigonal bipyramidal. A least-squares superposition of the C_α atoms of H119N and H119D CAIIs reveals that only slight changes in the position of solvent molecule SOL2 would result in inner-sphere metal coordination (Figure 6, Table 2). Therefore, it is possible that the tendency of zinc coordination geometry to change from tetrahedral (native CAII) to partially (H119D CAII) or fully (H119N CAII) trigonal bipyramidal results in comparable decreases in esterase activities mea-

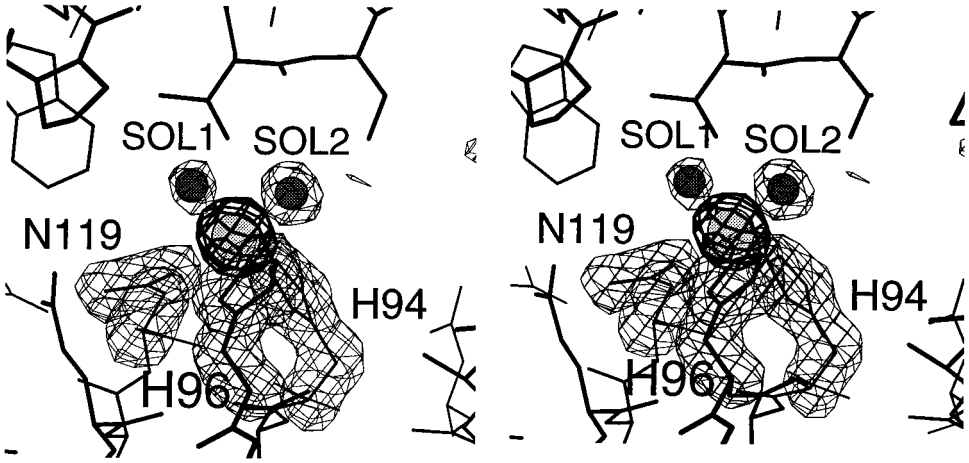

FIGURE 5: Difference electron density map of H119N CAII, generated with Fourier coefficients $|F_o| - |F_c|$ and phases calculated from the final model less the atomic coordinates of zinc ligands H94, H96, N119, and two zinc-bound solvent molecules. The map (thin lines) is contoured at 3.5σ; refined atomic coordinates are superimposed. Note that the metal coordination geometry in this variant is trigonal bipyramidal: N119 and SOL2 are apical ligands, and H94, H96, and SOL1 are equatorial ligands. The thick lines represent a difference map omitting the zinc ion from the structure factor calculation and contoured at 10σ.

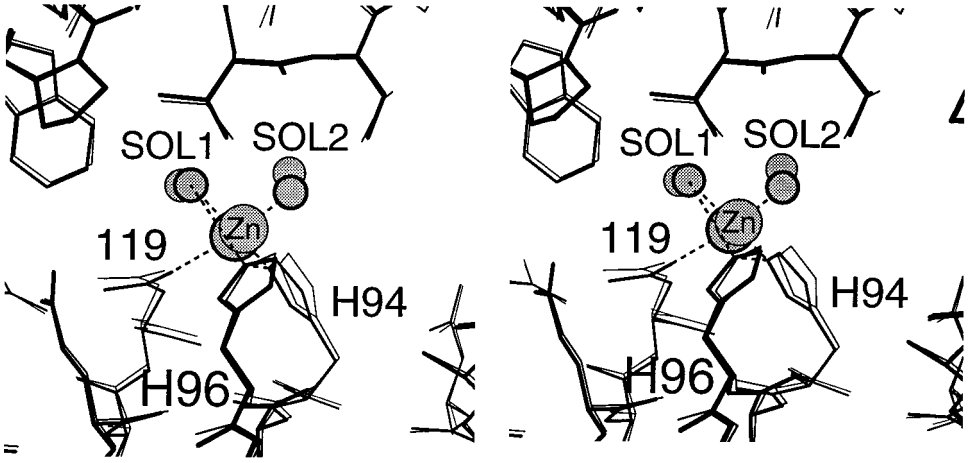

FIGURE 6: Least-squares superposition of the zinc binding sites of H119D CAII (thin lines; Kiefer et al., 1993) and H119N CAII (thick lines). The substitution of aspartate or asparagine for H119 results in a pentacoordinate zinc ion with trigonal bipyramidal coordination geometry, but in the H119D variant the D119 carboxylate−metal coordination is relatively weak with a Zn^{2+}−O separation of 2.8 Å.

sured for these variants. Apparently, the bulky histidine imidazole ligands help to maintain a low coordination number for zinc in the native enzyme active site.

In contrast to results with the asparagine/aspartate variants, the esterase activities of CAII variants containing neutral histidine → glutamine substitutions are increased more than 10-fold compared to variants containing the corresponding negatively charged histidine → glutamate substitutions (Table 3; Kiefer & Fierke, 1994). This result is consistent with the proposal that the catalytic transition state is destabilized by additional negative charge in the zinc coordination polyhedron (Kiefer & Fierke, 1994; Christianson & Fierke, 1996). However, the decreased activities of the H94E and H119E CAII variants may also be caused by structural perturbations in the active site, such as those resulting from the disorder of the E94 side chain observed in the X-ray crystal structure (Xue et al., 1994). The X-ray crystal structure of H119Q CAII reveals a tetrahedral zinc coordination polyhedron in which the O_ϵ atom of Q119 substitutes for the N_δ atom of H119 with good coordination stereochemistry (Figure 7); the side chain NH_2 group of Q119 maintains a hydrogen bond interaction with the side chain of E117. The zinc ion moves approximately 0.6 Å from its position in the native enzyme in a direction away from the longer Q119 side chain and zinc-bound hydroxide moves 1.0 Å from its position in the native enzyme (Figure 8). These structural changes are apparently small enough to sustain near-normal levels of esterase activity but large enough to decrease CO_2 hydration and sulfonamide affinity 16-fold.

The correlation of structure with esterase activity in histidine → glutamine variants reflects the role of the protein in modulating the pK_a—and hence the reactivity—of the catalytic nucleophile, zinc-bound hydroxide. The pK_a of zinc-bound water is either unperturbed (H119Q CAII) or increased 0.5−1.7 units in H119N, H94N, and H94Q CAIIs due to the histidine → asparagine and histidine → glutamine substitutions (Table 3). This is in contrast to the larger pK_a increases ($\geq$2.7 units) resulting from coordination of a negatively charged ligand, as observed in H94C and H94D CAIIs (Table 3; Kiefer & Fierke, 1994). The ΔpK_a values resulting from histidine → negatively charged ligand substitutions are attenuated if the engineered metal−ligand bond is quite long (e.g., the carboxylate−zinc separation in H119D CAII is 2.8 Å) or if the side chain swings away to allow an additional water molecule access to the metal coordination sphere (e.g., as in H96C CAII; Ippolito & Christianson, 1994). Therefore, the electrostatic environment around the zinc site modulates the pK_a of zinc-bound water. It is clear

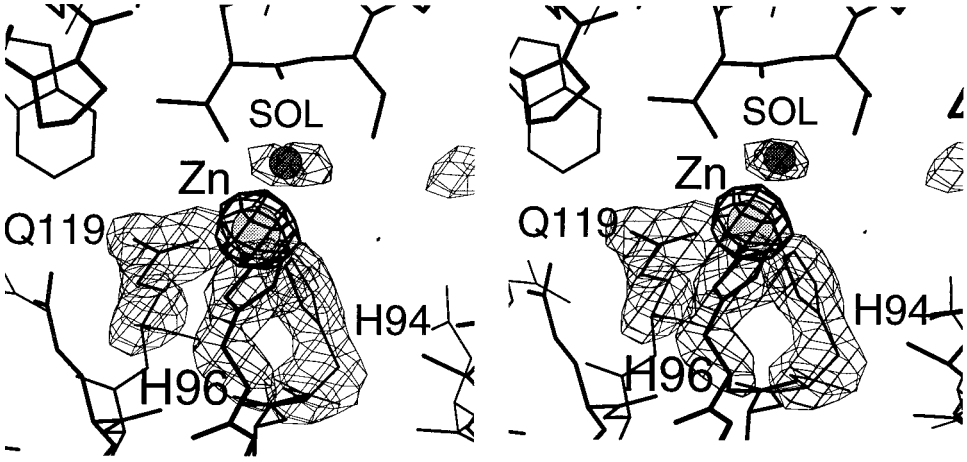

FIGURE 7: Difference electron density map of H119Q CAII, generated with Fourier coefficients $|F_o| - |F_c|$ and phases calculated from the final model less the atomic coordinates of zinc ligands H94, H96, Q119, and zinc-bound hydroxide. The map is contoured at 3.5σ; refined atomic coordinates are superimposed. Note that zinc coordination remains tetrahedral in this variant. The thick lines represent a difference map omitting the zinc ion from the structure factor calculation and contoured at 10σ.

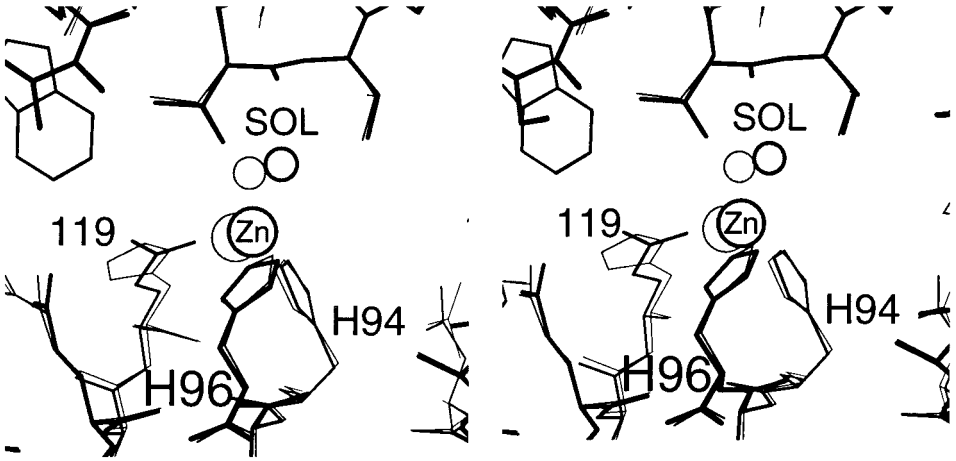

FIGURE 8: Least-squares superposition of H119Q (thick lines) and native (thin lines) CAIIs. Note that tetrahedral zinc coordination geometry is maintained in the variant.

that the neutral histidine ligands are crucial for maintaining sufficient positive charge on zinc to stabilize the zinc−hydroxide species, which results in a depressed pK_a for zinc-bound water and high catalytic efficiency at neutral pH.

CO_2 Hydration. To further probe the effects of histidine → carboxamide ligand substitutions on the reactivity of zinc−hydroxide, we measured the catalytic parameters for the physiologically important CO_2 hydration reaction. To obtain the pH-independent kinetic parameters, CO_2 hydrase activity was measured at a pH significantly above the pK_a of zinc-bound water (Tables 3 and 4). For three variants, H119N, H119Q, and H94N CAIIs, moderate decreases (11−24-fold) were observed in the values of k_{cat}/K_M for CO_2 hydration. For wild-type CAII, k_{cat}/K_M measures the formation of the transition state for CO_2 hydration compared to the ground state of CAII and unbound substrate (Lindskog, 1984; Rowlett, 1984). Therefore, these data indicate that the histidine → carboxamide substitutions decrease the reactivity of zinc-bound hydroxide without significantly elevating the pK_a of zinc−water. A likely explanation for this result is that the position or geometry of the metal site is slightly altered so that the active site nucleophile is no longer in an optimal position to react; this is consistent with the X-ray crystal structures of H94N, H119N, and H119Q CAIIs as described in the previous section. The reductions in CO_2 hydrase activity measured for these variants are 3−9-fold larger than the corresponding reductions of esterase activity, further suggesting that activity losses are caused more so by structural effects than electrostatic effects on the reactivity of zinc-bound hydroxide. Additionally, the observed 2−7-fold decreases in k_{cat}/K_M for the variants with carboxamide substitutions compared to the k_{cat}/K_M for the variants with the corresponding carboxylate substitutions are much smaller than the differences in the pK_a of the zinc−water. One variant, H94Q CAII, has esterase, hydrase, and

Table 4: Steady-State Kinetic Parameters for CO_2 Hydration Catalyzed by CAII Variants[a]

CAII variant	k_{cat} ($s^{-1} \times 10^{-4}$)	K_M (mM)	k_{cat}/K_M[b] ($\mu M^{-1}\ s^{-1}$)
wild type[c]	100	8.2	110 (110)
H94N[d]	3.2 ± 0.3	8.9 ± 2.6	3.6 ± 0.6 (4.5)
H94Q	0.90 ± 0.21	28 ± 10	0.32 ± 0.04 (0.42)
H94E	0.098 ± 0.003	4 ± 1	0.21 ± 0.02
H119N	4.8 ± 0.5	5 ± 2	9.3 ± 2.2 (10.5)
H119Q	≥34[e]	≥50[e]	6.8 ± 0.7 (6.9)
H119E	≥0.2[e]	≥50[e]	0.045 ± 0.005

[a] Measured in 50 mM TAPS, pH 9.0, and 25 μM *m*-cresol purple, 25 °C, with ionic strength maintained at 0.1 M by addition of sodium sulfate. [b] k_{cat}/K_M corrected for the pK_a of the zinc−water (Table 1) is shown in parentheses. [c] Taken from Kiefer and Fierke (1994). [d] Measured in 50 mM MOPS, pH 7.9, and 25 mM *p*-nitrophenol, 25 °C, with ionic strength maintained at 0.1 M by addition of sodium sulfate. [e] No curvature in a plot of rate versus [CO_2] up to 24 mM.

dehydrase activities (Tables 3 and 4; data not shown) that are significantly lower than any of the other variants with carboxamide side chains. This result indicates that the glutamine side chain is not a viable zinc ligand replacement for the N_ϵ atom of histidine at this position.

In wild-type CAII at high concentrations of buffer, k_{cat} for CO_2 hydration measures the intramolecular proton transfer between zinc−water and H64 (Silverman & Lindskog, 1988). Except for H119Q CAII, the k_{cat} values for variants with asparagine or glutamine substituted for one of the histidine zinc ligands decrease significantly (16−600-fold; Table 4). Since proton transfer between H64 and zinc−water occur via an ordered water chain (Håkansson et al., 1992), one possible explanation for the decreased k_{cat} values is that structural changes in the zinc binding site partially disrupt the active site water chain connecting these two groups. However, the three-dimensional structures of H94N, H119N, and H119Q CAIIs indicate that this postulated proton translocation pathway is intact when compared with the native structure (Håkansson et al., 1992). Catalytic proton transfer in CAII can be disrupted in three different ways: (1) altering the position and/or mobility of the proton acceptor (Tu et al., 1989; Krebs et al., 1991; Liang et al., 1993), (2) varying the pK_a of either the donor or acceptor group (Forsman et al., 1988; Engstrand et al., 1992**;** Silverman et al., 1993; Ren et al., 1995), and (3) blocking the formation of a hydrogen bonded solvent network—i.e., a "proton wire"—between donor and acceptor group (Jackman et al., 1996; Scolnick & Christianson, 1996). In the series of histidine → asparagine and histidine → glutamine zinc site variants, it appears that reduced proton transfer rate constants between zinc-bound solvent and H64 result from a combination of slight changes in the pK_a of zinc-bound water, as well as altered positions for zinc-bound water (due to the movement of zinc and/or the addition of a second coordinated water molecule).

Inhibitor Binding. Sulfonamides are specific inhibitors of carbonic anhydrase that have been proposed to mimic the transition state for CO_2 hydration (Kumar et al., 1976). The X-ray crystal structures of CAII−sulfonamide complexes show that the ionized nitrogen atom of the inhibitor coordinates to zinc and displaces the zinc-bound water (Vidgren & Liljas, 1990; Vidgren et al., 1993). In order to further investigate the effects of histidine → carboxamide ligand substitutions on the stabilization of the transition state, we measured the affinity of these CAIIs for two different sulfonamide inhibitors, DNSA and AZA. The dissociation constants for DNSA binding to CAII variants were measured as an increase in fluorescence at 470 nm due to fluorescence energy transfer between CAII tryptophans and DNSA (Chen & Kernohan, 1967; Table 3). The dissociation constants for AZA (Table 3) were measured by competition with dansylamide as a decrease in fluorescence due to the disappearance of E·DNSA and the concomitant formation of an E·AZA complex. In all cases, the data are well-described by a single observed dissociation constant. Sulfonamide binding to wild-type CAII is pH independent from 7−9; binding decreases at both high and low pH, reflecting ionization of the sulfonamide moiety (p$K_a \approx 9$) and the zinc-bound water molecule (Kernohan, 1966; Lindskog & Thorslund, 1968). The pK_a of zinc-bound water increases (≥0.5 pH unit) in H94Q and H119N CAIIs, which alters the pH dependence of sulfonamide binding; the values listed in parentheses in Table 3 are corrected for this difference.

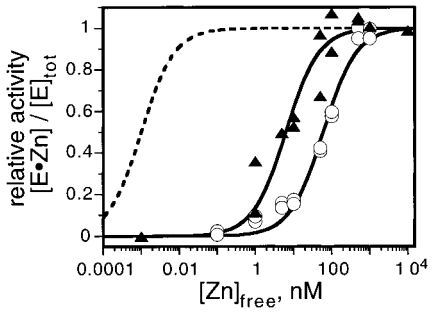

FIGURE 9: Measurements of the zinc dissociation constant of H119Q (○), H94Q (▲), and wild-type (dashed line). CAII variants (0.2 mL of 60 μM) were dialyzed against 500 mL of zinc/dipicolinate metal ion buffers (0−85 μM total zinc/0.1−2 mM dipicolinate) in 10 mM MOPS, pH 7.0. After 9−24 h of incubation at 30 °C, the fraction of zinc-bound enzyme, $[E\cdot Zn]/[E]_{tot}$, was determined from the relative specific activity for PNPA hydrolysis in 50 mM TAPS, pH 8.5, for H119Q and wild-type CAII and 50 mM TAPS, pH 9.4 for H94Q CA11. The dissociation constant was calculated using eq 4.

The sulfonamide affinities of the CAII variants with histidine → asparagine or glutamine substitutions are similar to those of wild-type CAII (Table 3); they range from binding 5-fold more tightly (H94N CAII) to 38-fold more weakly (H119Q CAII). The X-ray crystal structure of the H94N CAII·AZA complex reveals identical inhibitor binding interactions to those observed in the native CAII·AZA complex (data not shown). An additional interaction present in the variant but not in the native enzyme is a possible weak hydrogen bond between the carboxamide NH_2 group and one sulfonamide oxygen of the inhibitor (O···N separation = 3.4 Å) that might contribute to the increased affinity. Differences in inhibitor affinity among the greater series of CAII variants likely reflect minor structural differences in the active site of each variant that accommodate the amino acid substitution.

Carboxamide ligand variants of CAII bind sulfonamides 50−10^5-fold more tightly than the corresponding carboxylate ligand variants (Table 3; Kiefer & Fierke, 1994). In the most extreme example, the K_{AZA} for H94D CAII compared to H94N CAII decreases from 207 to 0.002 μM. This indicates that the electrostatic interaction between the negatively charged sulfonamide nitrogen and the positively charged zinc ion is critical for the high affinity of sulfonamide inhibitors. These data, combined with the effects of ligand substitution on the pK_a of zinc-bound water, clearly demonstrate that the positive charge on the zinc ion is crucial for stabilizing the binding of anions to the active site of CAII.

Zinc Affinity. In order to elucidate the effects of the histidine → carboxamide substitutions on metal affinity, the zinc dissociation constant, K_{Zn}, was determined for each variant by equilibrium dialysis (Figure 9). At high concentrations of zinc (≥100 nM), the stoichiometry of zinc bound to CAII is larger than 1, indicating the presence of multiple zinc binding sites. This additional zinc binding site(s) is also observed in wild-type CAII at high zinc concentrations (data not shown). To correctly measure the dissociation constant of the active site zinc, the fraction of active sites containing a bound zinc ion ($[E\cdot Zn]/[E]_t$) was determined by measuring the relative specific activity for PNPA hydrolysis (Figure 9). The K_{Zn} values are listed in Table 5 and demonstrate that the zinc affinity is substantially

Table 5: Zinc Dissociation Constants and Dissociation Rate Constants for CAII Variants

CAII variant	K_{Zn}[a] (nM)	k_{off}[b] (min^{-1})	k_{on}[c] ($\mu M^{-1}\ s^{-1}$)	$t_{1/2}$[d] (min)
wild type[e]	0.0008 ± 0.0001	$(5.0 \pm 1.0) \times 10^{-6}$	0.10	1.4×10^5
H119N	11 ± 4	0.148 ± 0.010	0.22	4.7
H119Q	69 ± 11	0.096 ± 0.018	0.023	7.2
H94N	40 ± 15	0.075 ± 0.011	0.031	9.2
H94Q	8 ± 3	0.335 ± 0.188	0.70	2.1
H119D[f]	25 ± 7	0.17 ± 0.04	0.11	4.1
H94D[f]	15 ± 5	0.011 ± 0.0004	0.012	63
H94E[f]	14 ± 5	0.49 ± 0.24	0.58	1.4

[a] Measured by an equilibrium dialysis method at pH 7.0 in 10 mM MOPS, as described in the legend of Figure 9. [b] Measured by the time-dependent decrease in the PNPA esterase activity in the presence of 0.5 mM PNPA and 10 mM MOPS, pH 7.0, with 5 mM EDTA, as described in the legend of Figure 10. [c] Calculated from $k_{on} = k_{off}/K_{Zn}$, assuming a simple binding step. [d] Calculated from $t_{1/2} = \ln 2/k_{off}$. [e] Taken from Hunt and Fierke (1997). [f] Taken from Kiefer and Fierke (1994).

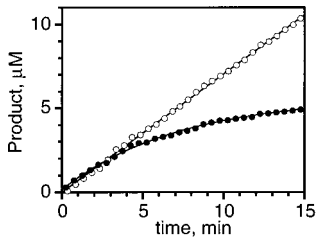

FIGURE 10: Measurement of the zinc dissociation rate constant of H119N CAII. The rate constant for zinc dissociation, k_{off}, was determined by diluting 1 μM H119N CAII into 0.5 mM PNPA and 10 mM MOPS, pH 7.0, with 5 mM EDTA to chelate zinc dissociating from the enzyme. Dissociation of zinc from CAII was monitored by the time-dependent decrease in the PNPA esterase activity, reflecting the concentration of enzyme-bound zinc (●). The k_{off} is calculated by fitting the data to eq 3. The initial activity of the zinc-bound enzyme was determined in the absence of the zinc chelator, EDTA (○).

diminished, 10^4-10^5-fold, into the nanomolar range. Nevertheless, these zinc affinities are comparable to those measured for the corresponding carboxylate substitutions for H94 and H119 CAII (Kiefer & Fierke, 1994; Table 5). This indicates that differences in zinc affinity are likely dominated by the structural changes in the zinc coordination polyhedron resulting from the deletion of a naturally evolved histidine ligand, rather than decreased metal−ligand interaction (Gurd & Wilcox, 1956). Analysis of the crystal structures of these variants suggests that the movement of the zinc ion from its position in the native enzyme (up to 1 Å) is the principal structural feature signaling diminished protein−zinc affinity.

The zinc dissociation rate constants, k_{off}, were measured by tracking the time-dependent decrease of PNPA hydrolysis activity in the presence of the zinc chelator, EDTA, that binds any dissociated zinc but does not catalyze dissociation of the zinc ion from wild-type CAII (Lindskog, 1982; Figure 10, Table 5). The zinc dissociation rate constants for all four CAII variants with carboxamide groups substituted in their metal coordination polyhedra increase about 10^4-10^5-fold, paralleling the decrease in the K_{Zn} and comparable to the values measured for variants with histidine → carboxylate substitutions (Kiefer & Fierke, 1994; Table 5). Assuming a simple binding step, the association rate constants can be calculated from K_{Zn} and k_{off} ($k_{on} = k_{off}/K_{Zn}$) and range from 10^4 to 10^6 $M^{-1}\ s^{-1}$. These values are comparable to the association rate constant measured for wild-type CAII under similar conditions (Table 5) and are much slower than the diffusion-controlled limit (Eigen & Hammes, 1963), which implies a two-step metal binding mechanism.

In one proposed mechanism (Scheme 2), two histidine ligands bind to the zinc rapidly to form the initial complex,

Scheme 2

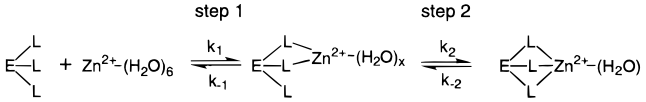

and then the rate-limiting step is the exchange of the third histidine ligand with the inner-sphere water to form the tetrahedral zinc binding site. Assuming that $k_{-1} \gg k_2$, k_{off} measures k_{-2} and k_{on} measures k_1k_2/k_{-1}. The slow k_{on} values observed in these asparagine/glutamine metal−ligand CAII variants, as well as in wild-type CAII, indicate that the second step of ligand exchange is rate-limiting. The 10^4-10^5-fold increase in k_{off} values is mainly caused by the faster dissociation of the third protein ligand, that is, k_{-2}.

Previous studies show that the complete removal of a single histidine ligand by replacing it with alanine greatly increases K_{Zn} to 100−1000 nM and increases k_{off} to >2 min^{-1}. Alanine variants H94A, H96A, and H119A CAIIs can only proceed through the first step, but not the second step, of metal binding as outlined in Scheme 2. The increased K_{Zn} and k_{off} values of these variants compared to the corresponding asparagine/glutamine or aspartate/glutamate variants indicate that a third protein ligand is required for high metal affinity. One might have assumed that negatively charged ligands, aspartate and glutamate, should lead to higher affinity for zinc than the neutral ligands, asparagine and glutamine, because charge−charge interactions are stronger than dipole−charge interactions. However, no such preferences are observed, perhaps because these substitutions are not perfectly isosteric with respect to metal coordination distances; e.g., in H119D CAII the $Zn^{2+}-O$ separation is 2.8 Å, whereas in H119N CAII this separation is 2.1 Å. The longer ligand−metal separation in H119D CAII may slightly attenuate the contribution of the electrostatic interaction to protein−zinc affinity. In general, the metal binding properties, k_{off}, K_{Zn}, and calculated k_{on}, have no distinguishable specificities for (1) the charge of the side chain, e.g., neutral asparagine or negatively charged aspartate, (2) the length of the side chain, e.g., asparagine or glutamine, or (3) the position of the substitution, 119 or 94. This suggests that the proper orientation and separation of metal ligands is the major determinant of zinc affinity in these CAII variants.

SUMMARY AND CONCLUSIONS

Asparagine and glutamine side chains substituted for zinc ligands H94 and H119 in single-point variants of CAII result in engineered protein−zinc binding sites with altered properties. These are the first neutral → neutral ligand substitutions

engineered into the zinc binding site of CAII, and the X-ray crystal structures of H94N, H119N, and H119Q CAIIs reveal that each carboxamide side chain coordinates to zinc through the side chain carbonyl oxygen. Metal coordination geometry remains tetrahedral in H119Q CAII, in which hydroxide ion is the fourth nonprotein zinc ligand as observed in the native enzyme. Surprisingly, zinc coordination geometry changes from tetrahedral to trigonal bipyramidal in H119N CAII due to the addition of a second water molecule to the inner sphere of metal coordination. Similar behavior is observed in H119D CAII, but the carboxylate oxygen of D119 exhibits an outer-sphere zinc−oxygen separation of 2.8 Å (Ippolito & Christianson, 1994). Metal coordination geometry in H94N CAII is also trigonal bipyramidal because of the bidentate binding mode of a Tris buffer molecule.

Functional measurements on this series of CAII variants indicate that the neutral ligand field provided by the protein optimizes the electrostatic environment for the catalytic function of the metal ion at neutral pH. The electrostatic environment of the metal ion is also a critical determinant of the high affinity of ionized sulfonamide inhibitors toward CAII. However, the electrostatic environment of the metal ion does not appear to play a key role in modulating protein−zinc affinity. Metal affinity is significantly compromised by all histidine → carboxamide ligand substitutions, and this may result from significant movements (up to 1 Å) of the zinc ion from its position in the wild-type enzyme, as well as the minor, associated movements of metal ligands and the surrounding residues that accommodate the ligand substitution.

In closing, it is compelling to consider that the bulky histidine ligands (especially H119) may play a role in disfavoring trigonal bipyramidal coordination geometry, and therefore stabilizing a low coordination number, for the active site zinc ion of native CAII. This would help depress the pK_a of zinc-bound solvent and increase its reactivity, trends that accompany decreasing coordination number (Bertini et al., 1990). This may explain the higher pK_a values measured for zinc-bound water in H94N, H94Q, and H119N CAIIs.

ACKNOWLEDGMENT

We thank Keith McCall and Mrinal Mahapatro for technical assistance.

REFERENCES

Alexander, R. S., Nair, S. K., & Christianson, D. W. (1991) *Biochemistry 30,* 11064−11072.

Alexander, R. S., Kiefer, L. L., Fierke, C. A., & Christianson, D. W. (1993) *Biochemistry 32,* 1510−1518.

Armstrong, J. M., Myers, D. V., Verpoorte, J. A., & Edsall, J. T. (1966) *J. Biol. Chem. 241,* 5137−5149.

Arnez, J. G. (1994) *J. Appl. Crystallogr. 27,* 649−653.

Bertini, I., Luchinat, C., Rosi, M., Sgamellotti, A., & Tarantelli, F. (1990) *Inorg. Chem. 29,* 1460−1463.

Brünger, A. T., Kuriyan, J., & Karplus, M. (1987) *Science 235,* 458−460.

Cavalli, R. C., Burke, C. J., Kawamoto, S., Soprano, D. R., & Ash, D. E. (1994) *Biochemistry 33,* 10652−10657.

Chen, R. F., & Kernohan, J. C. (1967) *J. Biol. Chem. 242,* 5813−5823.

Christianson, D. W., & Fierke, C. A. (1996) *Acc. Chem. Res. 29,* 331−339.

Coleman, J. E. (1967) *J. Biol. Chem. 242,* 5212−5219.

Coleman, J. E. (1984) *Ann. N.Y. Acad. Sci. 429,* 26−48.

Collaborative Computational Project No. 4 (1994) *Acta Crystallogr. D50,* 760−763.

Eigen, M., & Hammes, G. G. (1963) *Adv. Enzymol. 25,* 1−38.

Engstrand, C., Forsman, C., Liang, Z., & Lindskog, S. (1992) *Biochim. Biophys. Acta 1122,* 321−326.

Fierke, C. A., Calderone, T. L., & Krebs, J. F. (1991) *Biochemistry 30,* 11054−11063.

Forsman, C., Behravan, G., Jonsson, B.-H., Liang, Z.-w., Lindskog, S., Ren, X., Sanström, J., & Wallgren, K. (1988) *FEBS Lett. 229,* 360−362.

French, G. S., & Wilson, K. S. (1978) *Acta Crystallogr. A34,* 517−525.

Goldberg, J., Huang, H.-b., Kwon, Y.-g., Greengard, P., Nairn, A. C., & Kuriyan, J. (1995) *Nature 376,* 745−753.

Gurd, F. R. N., & Wilcox, P. E. (1956) *Adv. Protein Chem. 11,* 311−428.

Håkansson, K., Carlsson, M., Svensson, L. A., & Liljas, A. (1992) *J. Mol. Biol. 227,* 186−190.

Huang, C.-c., Lesburg, C. A., Kiefer, L. L., Fierke, C. A., & Christianson, D. W. (1996) *Biochemistry 35,* 3439−3446.

Hunt, J. A., & Fierke, C. A. (1997) *J. Biol. Chem. 272,* 20364−20372.

Hunt, J. B., Rhee, M., & Storm, C. B. (1977) *Anal. Biochem. 79,* 614−617.

Hunt, J. B., Neece, S. H., Schachman, H. K., & Ginsburg, A. (1984) *J. Biol. Chem. 259,* 14793−14803.

Ippolito, J. A., & Christianson, D. W. (1994) *Biochemistry 33,* 15241−15249.

Ippolito, J. A., Baird, T. T., Jr., McGee, S. A., Christianson, D. W., & Fierke, C. A. (1995) *Proc. Natl. Acad. Sci. U.S.A. 92,* 5017−5021.

Jackman, J. E., Merz, K. M., & Fierke, C. A. (1996) *Biochemistry 35,* 16421−16428.

Jones, T. A., Zou, J. Y, Cowan, S. W., & Kjeldgaard, M. (1991) *Acta Crystallogr. A47,* 110.

Jonsson, S.-H., Steiner, H., & Lindskog, S. (1976) *FEBS Lett. 64,* 310−314.

Kabsch, W. (1993) *J. Appl. Crystallogr. 24,* 795−800.

Kernohan, J. C. (1966) *Biochim. Biophys. Acta 118,* 405−412.

Khalifah, R. G. (1971) *J. Biol. Chem. 246,* 2561−2573.

Kiefer, L. L., & Fierke, C. A. (1994) *Biochemistry 33,* 15233−15240.

Kiefer, L. L., Ippolito, J. A., Fierke, C. A., & Christianson, D. W. (1993) *J. Am. Chem. Soc. 115,* 12581−12582.

Kiefer, L. L., Paterno, S. A., & Fierke, C. A. (1995) *J. Am. Chem. Soc. 117,* 6831−6837.

Kraulis, P. (1991) *J. Appl. Crystallogr. 24,* 946−950.

Krebs, J. F., Fierke, C. A., Alexander, R. S., & Christianson, D. W. (1991) *Biochemistry 30,* 9153−9160.

Krebs, J. F., Ippolito, J. A., Christianson, D. W., & Fierke, C. A. (1993) *J. Biol. Chem. 268,* 27458−27466.

Kumar, K., King, R. W., & Carey, P. R. (1976) *Biochemistry 15,* 2195−2202.

Kunkel, T. A. (1985) *Proc. Natl. Acad. Sci. U.S.A. 82,* 488−492.

Lesburg, C. A., & Christianson, D. W. (1995) *J. Am. Chem. Soc. 117,* 6838−6844.

Liang, Z., Xue, Y., Behravan, G., Jonsson, B. H., & Lindskog, S. (1993) *Eur. J. Biochem. 211,* 821−827.

Liljas, A., Kannan, K. K., Bergstén, P.-C., Waara, I., Fridborg, K., Strandberg, B., Carlbom, U., Järup, L., Lövgren, S., & Petef, M. (1972) *Nat. New Biol. 235,* 131−137.

Lindskog, S. (1982) *Adv. Inorg. Biochem. 4,* 115−170.

Lindskog, S. (1984) *J. Mol. Catal. 23,* 357−368.

Lindskog, S., & Thorslund, A. (1968) *Eur. J. Biochem. 3,* 453−460.

Lindskog, S., & Coleman, J. E. (1973) *Proc. Natl. Acad. Sci. U.S.A. 70,* 2505−2508.

Lindskog, S., & Liljas, A. (1993) *Curr. Opin. Struct. Biol. 3,* 915−920.

Ma, L., & Kantrowitz, E. R. (1994) *J. Biol. Chem. 269,* 31614−31619.

Ma, L., & Kantrowitz, E. R. (1996) *Biochemistry 35,* 2394−2402.

Ma, L., Tibbitts, T., & Kantrowitz, E. R. (1995) *Protein Sci. 4,* 1498−1506.

McPherson, A., Koszelak, S., Axelrod, H., Day, J., Williams, R., Robinson, L., McGrath, M., & Cascio, D. (1986) *J. Biol. Chem. 261*, 1969−1975.

Nair, S. K., Krebs, J. F., Christianson, D. W., & Fierke, C. A. (1995) *Biochemistry 34*, 3981−3989.

Nyborg, J., & Wonacott, A. J. (1977) in *The Rotation Method in Crystallography* (Arndt, U. W., & Wonacott, A. J., Eds.) pp 139−152, North Holland, Amsterdam.

Osborne, W. R. A., & Tashian, R. E. (1975) *Anal. Biochem. 64*, 297−303.

Read, R. J. (1986) *Acta Crystallogr. A42*, 140−149.

Ren, X., Tu, C., Laipis, P. J., & Silverman, D. N. (1995) *Biochemistry 34*, 8492−8498.

Rowlett, R. S. (1984) *J. Protein Chem. 3*, 369−393.

Sanger, F., Nicklen, S., & Coulson, A. R. (1977) *Proc. Natl. Acad. Sci. U.S.A. 74*, 5463−5467.

Scolnick, L. R., & Christianson, D. W. (1996) *Biochemistry 35*, 16429−16434.

Scolnick, L. R., Kanyo, Z. F., Cavalli, R. C., Ash, D. E., & Christianson, D. W. (1997) *Biochemistry 36*, 10558−10565.

Sillén, L. G., & Martell, A. E. (1964) *Stability constants of metal ion complexes*, Spec. Publ. No. 17, p 546, The Chemical Society, London.

Silverman, D. N. (1995) *Methods Enzymol. 249*, 479−503.

Silverman, D. N., & Lindskog, S. (1988) *Acc. Chem. Res. 21*, 30−36.

Silverman, D. N., Tu, C., Chen, X., Tanhauser, S. M., Kresge, A. J., & Laipis, P. J. (1993) *Biochemistry 32*, 10757−10762.

Sly, W. S., & Hu, P. Y. (1995) *Annu. Rev. Biochem. 64*, 375−401.

Smith, A. A., Carlow, D. C., Wolfenden, R., & Short, S. A. (1994) *Biochemistry 33*, 6468−6474.

Steiner, H., Jonsson, B.-H., & Lindskog, S. (1975) *Eur. J. Biochem. 59*, 253−259.

Sträter, N., Klabunde, T., Tucker, P., Witzel, H., & Krebs, B. (1995) *Science 268*, 1489−1492.

Tu, C. K., & Silverman, D. N. (1982) *Biochemistry 21*, 6353−6360.

Tu, C. K., Silverman, D. N., Forsman, C., Jonsson, B.-H., & Lindskog, S. (1989) *Biochemistry 28*, 7913−7918.

Vidgren, J., & Liljas, A. (1990) *Int. J. Biol. Macromol. 12*, 342−344.

Vidgren, J., Svensson, A., & Liljas, A. (1993) *Int. J. Biol. Macromol. 15*, 97−100.

Woolley, P. (1975) *Nature 258*, 677−682.

Xue, Y., Jonsson, B. H., Liljas, A., & Lindskog, S. (1994) *FEBS Lett. 352*, 137−140.

BI971296X